Reprinted from **APPLIED OPTICS,** Vol. 14, page 142, January 1975

Evaluation of Large Aberrations Using a Lateral-Shear Interferometer Having Variable Shear

M. P. Rimmer and J. C. Wyant

A variable shear lateral shearing interferometer consisting of two holographically produced crossed diffraction gratings is used to test nonrotationally symmetric wavefronts having aberrations greater than 100 wavelengths and slope variations of more than 400 wavelengths/diameter. Comparisons are made with results of Twyman-Green interferometric tests for wavefront aberrations of up to thirty wavelengths. The results indicate that small wavefront aberrations can be measured as accurately with the lateral-shear interferometer as with the Twyman-Green interferometer and that aberrations that cannot be measured at all with a Twyman-Green interferometer can be measured to about 1% accuracy or better.

Introduction

In a lateral shear interferometer (LSI), two superimposed displaced images of the wavefront under test are made to interfere with each other, i.e., an LSI compares a wavefront with a sheared version of itself. The fringes of a shearing interferogram are the loci of constant average wavefront slope over the shear distance. This is different from a wavefront measuring interferometer, such as a Twyman-Green, in that the fringes in a Twyman-Green interferogram are the loci of constant wavefront phase. Thus, shearing interferograms must be analyzed differently than Twyman-Green or LUPI (laser unequal path interferometer) interferograms. Recently a technique was developed that indicated that it is possible to obtain the wavefront as accurately from shearing interferograms as it is from Twyman-Green interferograms.[1,2] In many instances the advantages of an LSI over a LUPI more than compensate for the additional data processing required.

One advantage of an LSI over wavefront measuring interferometers, for example a Twyman-Green, is that the need for a reference wavefront is eliminated. Also, certain types of turbulence and vibrations cause less problems with an LSI than with other types of interferometers. Often the coherence requirements for the light source can be greatly reduced by using an LSI instead of a wavefront measuring interferometer. Another advantage that was being investigated during the course of this study was the ability to vary the effective sensitivity of the interferometer. The number of fringes in the lateral shear interferogram can be selected by varying the amount of shear. This provides the possibility of testing aspheric wavefronts without the use of null optics and without requiring data reduction of interferograms having a very large number of fringes.

The specific tasks involved in this study were as follows: (1) Design and fabricate a combination LUPI and LSI. The changeover from standard LUPI to LSI must require a minimum of adjustment. (2) Develop the analytic techniques and computer software necessary to evaluate the LSI interferograms. (3) Test both rotationally symmetric and nonsymmetric wavefronts using both the LSI and the LUPI, where feasible. Wavefronts having as much as 100-waves departure from a spherical wavefront were to be tested.

The results of this study demonstrate that small aberrations can be measured to about the same accuracy with .a shearing interferometer as with a LUPI, and large aberrations can be measured better with an LSI than with a LUPI. The LSI can currently be used for in-process testing of steep aspherics and for null tests.

Interferometer Description

A primary requirement in making the LSI-LUPI interferometer was that the changeover from LUPI to LSI operation must require a minimum of adjustment. Furthermore, since a lateral shear interferogram gives wavefront slope information only for the direction of shear,[1-3] the LSI must give two shearing interferograms, where the shears for the two interfer-

Both authors were with Itek Corporation, Optical Systems Division, Lexington, Massachusetts 02173 when this work was done. J. C. Wyant is now with the Optical Sciences Center, University of Arizona, Tucson, Arizona 85721.

Received 20 June 1974.

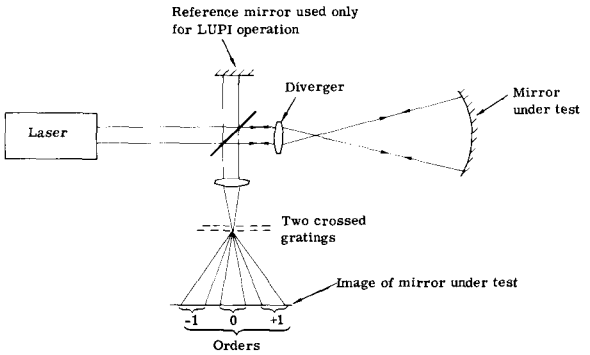

1. LSI-LUPI interferometer.

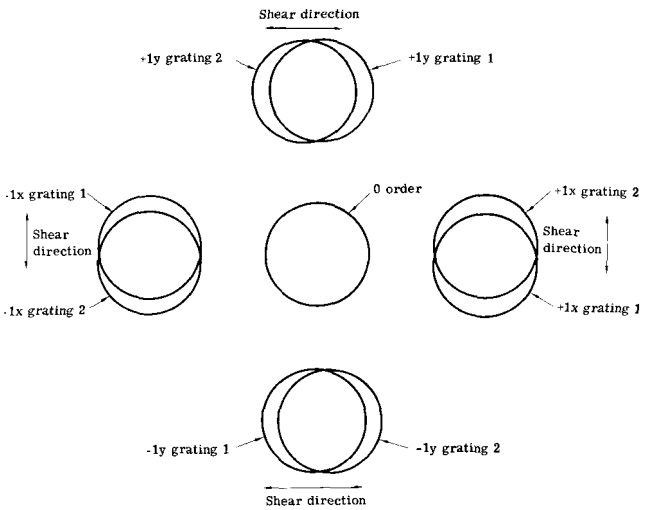

Fig. 2. Diffraction orders produced by two crossed gratings.

ograms are orthogonal. To reduce the effects of vibration and turbulence, the two shearing interferograms should be obtained simultaneously. A further requirement was the capability of varying the shear any desired amount from essentially zero shear up to half of the pupil diameter or more. The LSI described below, which uses two crossed holographically produced diffraction gratings to produce the shear, satisfies all these requirements.

Figure 1 shows a diagram of the LSI-LUPI interferometer. When the interferometer is being used as an LSI, an opaque card is placed between the beam splitter and the reference mirror. The light reflected off the test mirror back through the diverger is brought to focus either on or near the two crossed diffraction gratings, similar to a Ronchi test.[4-6] The requirement for no overlap of the zeroth and first-diffracted orders is that the grating spatial frequency is greater than the reciprocal of λf_{no}, where f_{no} is the f number of the converging cone of light of wavelength λ.

Figure 2 shows the diffraction orders produced by the two crossed diffraction gratings. Each grating gives four orders, ±1 in the x direction and ±1 in the y direction, as well as a zero order. Rotating a grating rotates the orders produced by the grating. If the two gratings are oriented identically, the corresponding orders produced by the two gratings will overlap and interfere with one another. If one grating is rotated with respect to the second grating, the orders will overlap less, i.e., a lateral shear is produced between the corresponding orders. A lateral shear interferogram will exist in the overlap region, the amount of shear being selected by rotating one grating relative to the second. The x orders and the y orders have shear in orthogonal directions.

The crossed diffraction grating used in the interferometer can be produced holographically by recording the interference of two plane waves, then rotating the recording medium 90° and making a second recording. If the recording medium is a photographic plate such as Agfa l0E56, the plates can be processed and bleached as described previously[7] to give 10% or more of the incident light in each of the shearing patterns. The relationship between shear and angular rotation of the diffraction grating can be easily calculated. If θ is the grating diffraction angle, α is the angle one grating is rotated with respect to the second grating, the percentage shear, i.e., the ratio of the shear distance to the beam radius is given by

$$\text{percentage shear} = 4f_{no}\tan\theta\sin(\alpha/2). \qquad (1)$$

For small values of θ and α this equation reduces to $2f_{no}\lambda\nu\alpha$, where ν is the spatial frequency of the grating lines.

Tilt between the two interfering wavefronts can be accomplished by either moving the gratings from the Gaussian focus or by changing the distance between the two gratings. This can be seen with the help of Fig. 3. Assume the light is coming to focus at point 0 a distance x_1 from the first grating and a distance x_2 from the second grating. Let one set of grating lines make an angle $-\alpha/2$ with respect to the y axis and the second set of grating lines an angle $+\alpha/2$ with respect to the y axis. The first grating diffracts part of the light so the light appears to be coming from point A, a vector displacement Δ_1 from point 0, while the

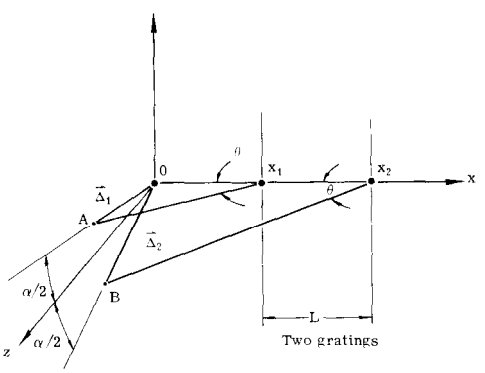

Fig. 3. Introduction of tilt between sheared wavefronts.

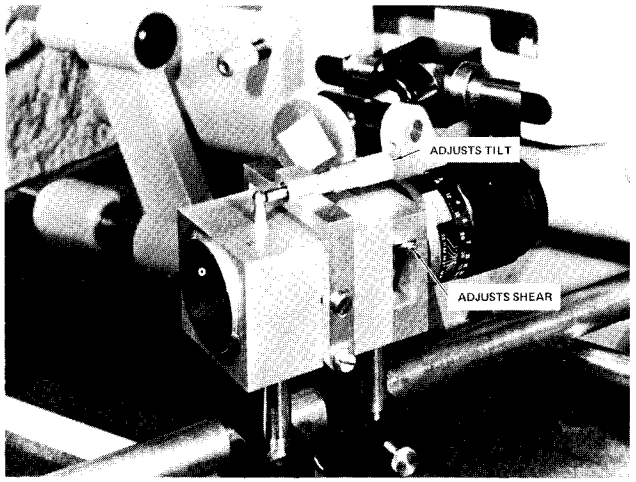

Fig. 4. LSI attachment to LUPI.

second grating diffracts some of the light that after diffraction appears to be coming from point B, a vector displacement Δ_2 from point 0. The two interfering wavefronts appear to be coming from foci separated an amount Δ, which is given by

$$\Delta = \Delta_2 - \Delta_1 = x_2 \tan\theta\left(-\sin\frac{\alpha}{2}\hat{j} + \cos\frac{\alpha}{2}\hat{k}\right) - x_1 \tan\theta\left(\sin\frac{\alpha}{2}\hat{j} + \cos\frac{\alpha}{2}\hat{k}\right) = \tan\theta\left[-(2x_1 + L)\sin\frac{\alpha}{2}\hat{j} + L\cos\frac{\alpha}{2}\hat{k}\right], \quad (2)$$

where L is the grating spacing. It should be noted that by varying the grating spacing L, the orientation of the fringes can be selected.

Experimental Setup

Figure 4 shows the grating lateral shear interferometer used to obtain the results shown in this paper. A high quality 135-mm, focal-length lens is mounted on the front of the interferometer to focus a collimated beam in the vicinity of the 200-line/mm gratings. The two gratings can be rotated with respect to one another by moving the small lever shown on the side of the interferometer. The tilt between the interfering wavefronts can be varied by adjusting the micrometer shown which varies the spacing between the gratings.

The LSI attachment was placed in the output beam of an Itek LUPI as shown in Fig. 5. The flipper shown on the LUPI controls an opaque screen that blocks out the reference beam when the interferometer is being used as an LSI. To switch from LSI operation to LUPI operation all that needs to be done is to move the opaque screen out of the reference beam. The interference between the reference beam and the zero order from the grating gives the LUPI interferogram.

Figure 6 shows a diagram of the setup used to obtain a known aspheric wavefront having as many as 100-waves departure from the best fitting spherical wavefront. The actual setup is shown in Fig. 5. The plane parallel plate is tilted a known amount to select the amount of wavefront aberration. The system is ray traced to determine the theoretical amount of wavefront aberration.

Interferograms

Using the setup shown in Fig. 6, interferograms were taken for tilts of the plane parallel plate up to 30° in steps of 5°. In addition, interferograms were taken with the plate removed in order to calibrate the sphere. These measurements were subsequently subtracted from the results obtained with the plate in place. The nature of the aberration introduced by the tilted plate is mostly astigmatism with some coma and spherical aberration. Figure 7 shows the relationship between peak-to-peak aberration and plate tilt. About 120 wavelengths of aberration were obtained for a 30° tilt of the plate. No usable LUPI interferograms were obtained for tilts greater than 15° because the fringe density became too high.

Figures 8 and 9 show the LUPI and LSI interferograms for plate tilts of 0° and 15°. The image of a square grid which was placed on the spherical mirror was used for reference purposes. Four intersection points were used for scaling the digitized interfero-

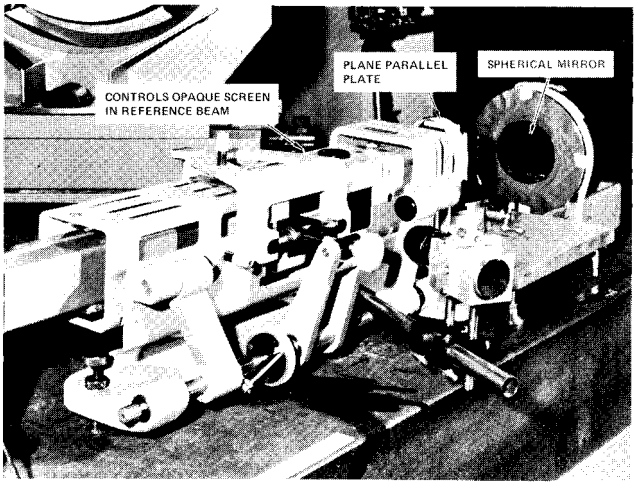

Fig. 5. LUPI and LSI.

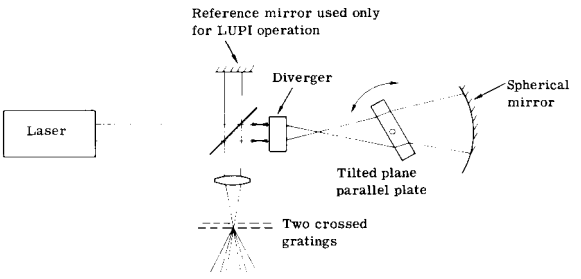

Fig. 6. Experimental setup used to obtain nonsymmetric aspheric wavefront.

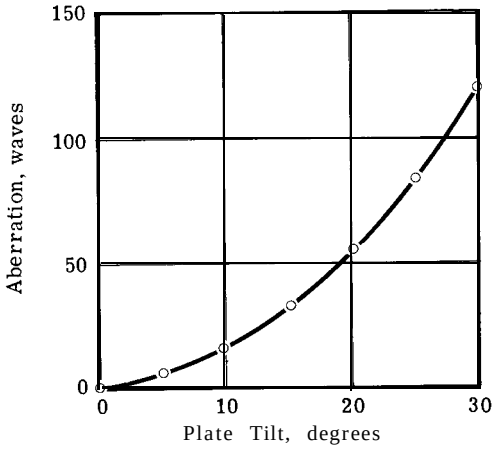

Fig. 7. Aberration vs plate tilt.

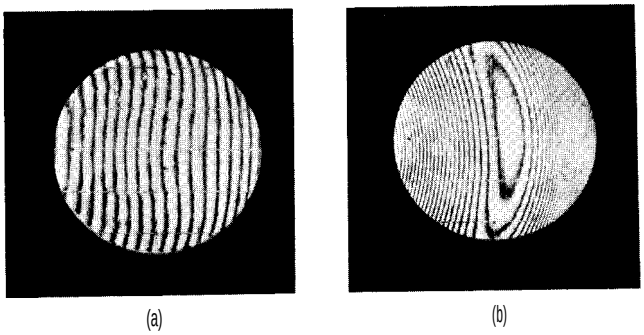

Fig. 8. LUPI interferograms: (a) plate tilt = 0°; (b) plate tilt = 15°.

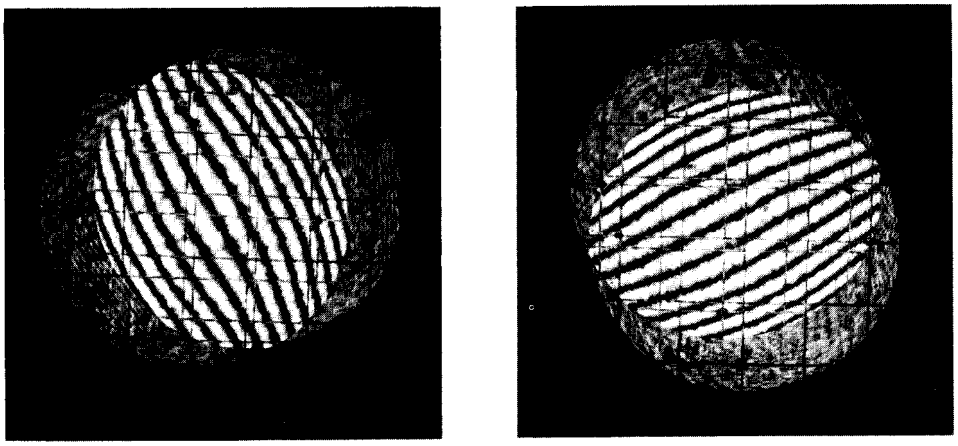

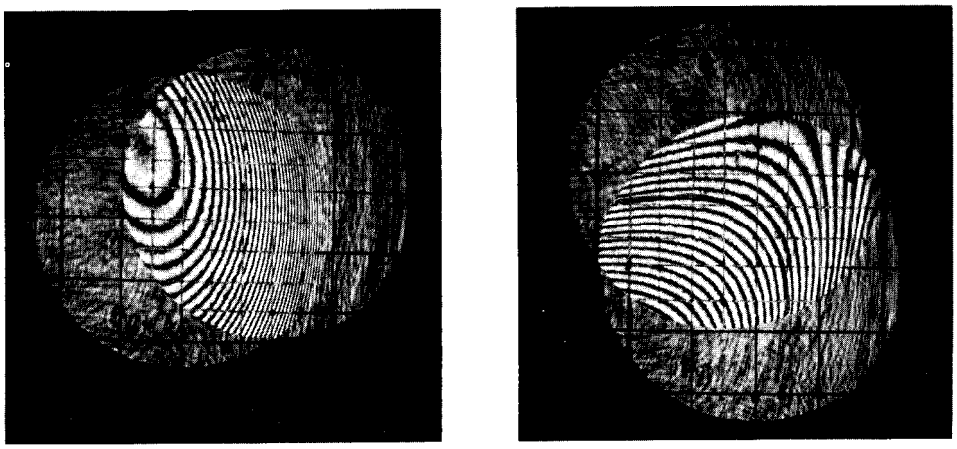

Fig. 9. LSI interferograms: (a) plate tilt = 0°, shear = 0.36; (b) plate tilt = 15°, shear = 0.63.

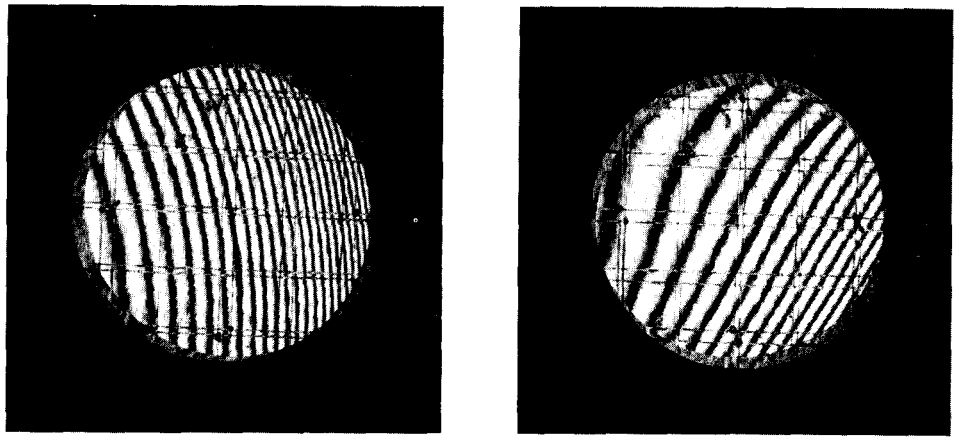

(a)

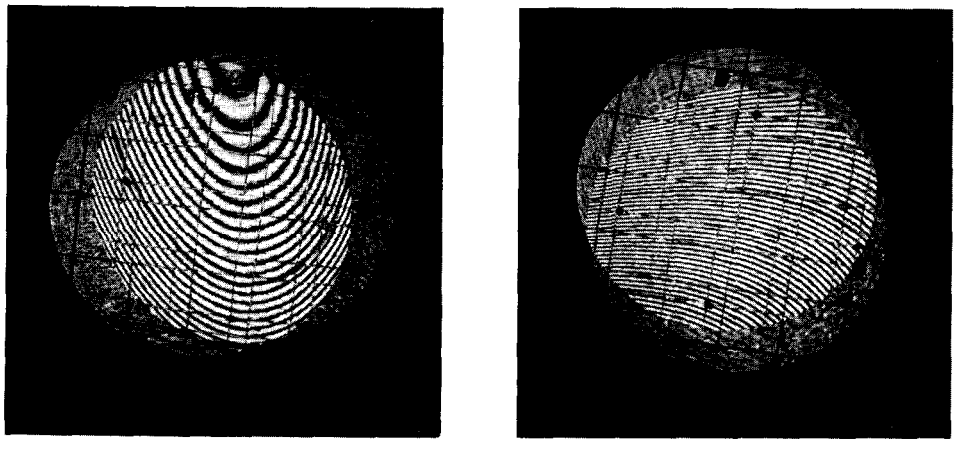

(b)

Fig. 10. LSI interferograms for plate tilt of 20°: (a) shear = 0.09; (b) shear = 0.30.

grams to a common coordinate system. In the LSI interferograms two images of the grid appear. Corresponding intersection points were used to calculate the shear. For the 0° tilt the shear is 0.36, given as a fraction of the aperture radius, and for the 15° tilt it is 0.63. The fringe density increases as the aberration increases and as the shear increases. Figures 10 and 11 show some of the other pairs of LSI interferograms obtained. The interferograms for a 20° tilt are shown for two different shear values.

Analysis

The interferograms were digitized with a two-coordinate precision measuring engine (David W. Mann Co., Hand Comparator, model 829C) having a digital output with a least count of 1 μm. This was attached to an IBM 026 keypunch to give digital data in a form suitable for the computer. These data consist of the coordinates of the centers of the fringes, along with the corresponding order of the fringe, at about 200 points approximately uniformly distributed over the interferogram. In addition, the coordinates of the intersections of selected grid lines were digitized. These were used to align and scale the data from each interferogram to a common coordinate system and to calculate the values of the shear.

The fringe data were fit to Zernike polynomials.8 The order to which the data must be fit depends on the nature of the data. The goal is to get a good representation of the data without fitting noise as well. This can usually be done by fitting to successively higher orders and stopping when there is no further significant reduction in the rms residual error.9 The LUPI interferograms were fit to order 6. No further analysis was required to obtain the wavefront except to remove the tilt and focus introduced by the interferometer. The LSI interferograms were fit to order 5. In general, if the LSI interferograms are fit to order k - 1, there will be $M = k(k + 1)/2$ coefficients for each. The resulting wavefront will be of order k and will be represented by $N = (k + 1)(k + 2)/2$ terms.

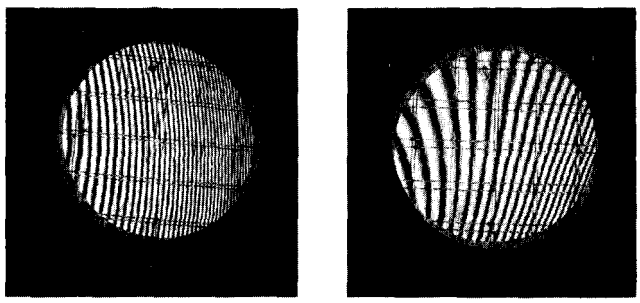

Fig. 11. LSI interferograms: plate tilt = 30°, shear = 0.09.

If the wavefront to be found is $W(x,y)$, it is assumed that the two shearing interferograms represent $W(x + S,y) - W(x,y)$ and $W(x,y + T) - W(x,y)$, where S and T are the shear values in x and y, respectively. Since the two shearing wavefronts will not be entirely consistent because of noise, the criterion used for averaging out the effects of this noise is that the reconstructed shearing data from the final wavefront match the measured shearing wavefronts as well as possible in the least-squares sense. The mathematical procedure is summarized as follows.

Define the following matrices, where the size of the matrix *is* given in parentheses. Details of the matrices are given in the Appendix.

a Coefficients of the x-shear data (M X 1).

b Coefficients of the y- shear data (M X 1).

c Coefficients of the unknown wavefront which are to be found (N X 1).

α Matrix relating the coefficients of a wavefront to the coefficients of the corresponding x shear (M X N). For example, if u and v are coefficients of a wavefront and its corresponding shearing data, $v = \alpha u$.

β Matrix similar to (α for the y shear (M X N).

G Diagonal matrix used to calculate the variance of a wavefront (M X M). For example, if u is the coefficients of a wavefront, the variance is $u^T Gu$ (T = transpose).

The differences between the measured shearing interferograms and those obtained from the unknown wavefront are $a - \alpha c$ and $b - \beta c$ for the two shears, respectively. The variance of this difference is

$$V = (\mathbf{a} - \alpha\mathbf{c})^T G(\mathbf{a} - \alpha\mathbf{c}) + (\mathbf{b} - \beta\mathbf{c})^T G(\mathbf{b} - \beta\mathbf{c}). \quad (3)$$

By equating the derivative of V with respect to c to zero, a least-squares solution for c may be found. This is

$$\mathbf{c} = Q^{-1}\mathbf{d}, \quad (4)$$

where

$$Q = \alpha^T G\alpha + \beta^T G\beta, \quad (5)$$

$$\mathbf{d} = \alpha^T G\mathbf{a} + \beta^T G\mathbf{b}. \quad (6)$$

In the shearing interferometer used for this study, the two gratings used to produce the shear were slightly separated. This produced a tilt in each shearing interferogram that was in a direction orthogonal to the shear. Thus, the x and y shearing interferograms had the terms Py and -Px, respectively, added to them. Since these terms cannot result from any contribution from wavefront, their effect can be added to Eq. (3) and the coefficient P solved for (note that if the signs were the same, extraneous astigmatism would be introduced into the solution for the wavefront).

Results

Wavefront values were obtained from the LUPI interferograms, the LSI interferograms, and a ray trace evaluation of the test setup. The LUPI results for the test with no plate were taken to represent the errors of the spherical mirror, and these were subtracted from all interferometric valuations where the plate was present. A summary of results is given in Table I. In taking differences between the interferometric measurements and the ray trace evaluation, differential adjustments in position, orientation, and scale of one wavefront with respect to the other were introduced to match them as closely as possible. This was to account for slight differences in the coordinate systems of the two wavefronts. A differential adjust-

Table I. RMS and Peak-to-Peak Values

Plate tilt (degrees)	Shear (fraction of aperture radius)	Comparison of rms and peak-to-peak values						Difference between measured and ray-traced wavefronts			
		Ray trace		LUPI		LSI		LUPI		LSI	
		rms	P-P	rms	P-P	rms	P-P	rms	P-P	rms	P-P
0	0.36	0.157	0.74	0.163	0.80	0.170	0.85	0.027	0.15	0.042	0.31
5	0.30	0.961	5.43	0.958	5.33	1.063	5.88	0.024	0.16	0.040	0.30
10	0.30	2.898	16.01	2.847	15.69	3.129	17.48	0.034	0.33	0.048	0.36
15	0.63	6.067	32.38	3.913	30.14	6.002	31.55	0.159	1.90	0.069	0.74
20	0.09	10.534	54.82			10.228	53.57			0.060	0.48
20	0.17	10.534	54.82			10.234	52.31			0.122	0.71
20	0.30	10.534	54.82			10.139	32.94			0.107	0.51
25	0.09	16.364	83.59			16.103	82.60			0.082	0.63
30	0.09	23.749	119.60			23.127	118.50			0.246	2.02

Note: All rms and P-P values are in wavelengths of 0.6328 μ.

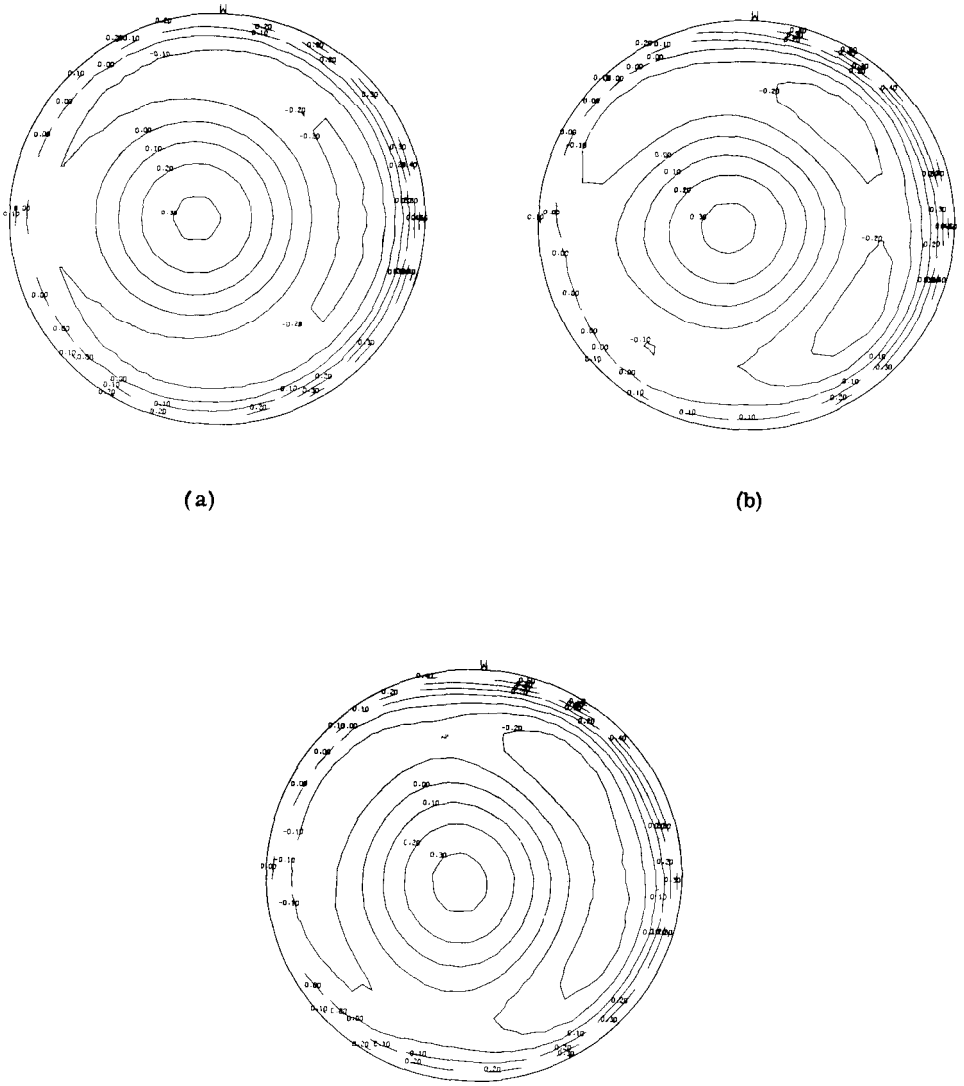

Fig. 12. Contour plots for plate tilt of 0° (contour intervals = 0.1 λ): (a) raytrace; (b) LUPI; (c) LSI.

ment in the tilt of the plate was also introduced to account for errors in the measurement of this parameter.

Figures 12 and 13 show contour maps for the predicted and measured wavefronts for plate tilts of 0° and 5°. Contour maps for the larger tilts would not show significant differences since the aberrations are too large.

It can be seen from the results at 0° orientation of the plate that there is some asymmetry in the wavefront that nominally should not be there. This is due to a tilt of the plate of 0.6°. Experimentally, the initial configuration of the plate was not known accurately. However, changes from this initial position were known to within 2 min of arc. The initial position of 0.6° was determined from the amount of coma in the LUPI test. Thus, the ray trace results are at values of 0.6°, 5.6°, 10.6°, etc., instead of 0, 5, 10, etc.

A major source of error in these results is in the measurement of the shear value. The percentage error in the shear measurement results in approximately the same percentage error in the wavefront. This error predominates for large aberrations. Another source of error is in the representation of the data by polynomials. This error becomes larger as the shear is reduced. An estimate of the error in the wavefront measurement from these two sources is shown in Fig. 14 for wavefronts of the type measured. Additional sources of error include registration of the two interferograms, aberration due to the grating, distortion of the fringe pattern due to the first order angle from the grating and the effect of the focusing lens.

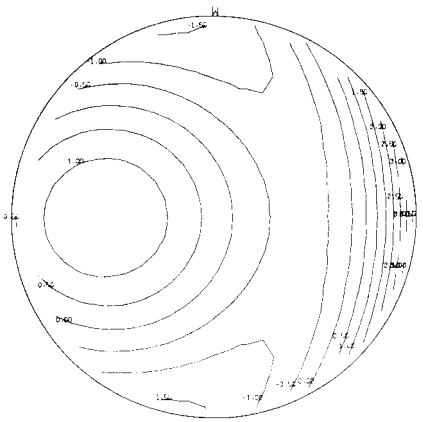

(a)

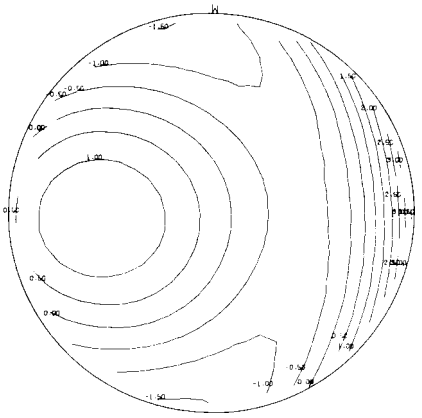

(b)

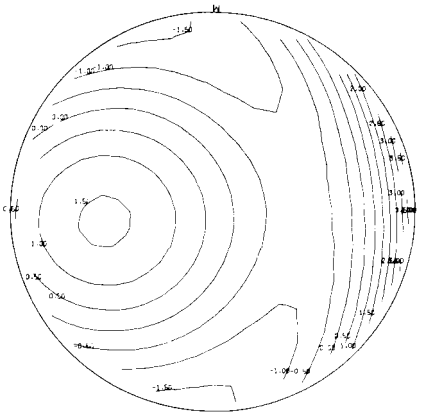

(c)

Fig. 13. Contour plots for plate tilt of 5°(contour intervals = 5λ): (a) raytrace; (b) LUPI; (c) LSI.

Conclusions

The combination LSI-LUPI interferometer designed and fabricated for this study fulfilled all the requirements and is exceedingly easy to operate. The changeover from LUPI operation to LSI operation only requires moving an opaque screen to block out the reference beam. The crossed diffraction gratings give two interferograms having orthogonal shear, simultaneously. The amount of shear can be easily adjusted to any desired amount by rotating one grating with respect to the second grating.

The analytic techniques for determining wavefront shape from digitized shearing interferograms have been demonstrated on wavefronts with more than 100 waves of aberration. It has been shown that the

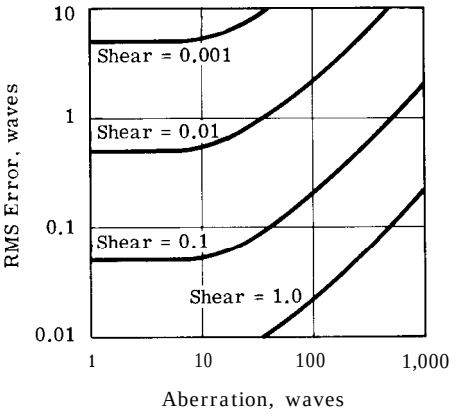

Fig. 14. Estimated error vs aberration.

LSI is more accurate than the LUPI for large wavefront aberrations and can measure wavefronts that cannot be measured at all with a LUPI. For small wavefront aberrations, the LSI can be as accurate as the LUPI. Shearing interferometry should prove very useful for in-process testing of steep aspherics and null testing.

Appendix

An expansion of a wavefront W in Zernike polynomials to order k has the general form

$$W(r,\theta) = \sum_{n=0}^{k}\sum_{m=0}^{n} A_{nm} R_n^{n-2m} \begin{Bmatrix}\sin\\ \cos\end{Bmatrix} (n-2m)\theta, \qquad (7)$$

where the sin function is used for $n - 2m > 0$ and the cos function for $n - 2m \le 0$. (r, θ) are polar coordinates in the unit circle, and R_n^{n-2m} are the radial polynomials defined by

$$R_n^{n-2m} = \sum_{s=0}^{m} (-1)^s \frac{(n-s)!}{s!(m-s)!(n-m-s)!} r^{n-2s}. \qquad (8)$$

A_{nm} are the coefficients of the Zernike polynomials. The variance of the wavefront is given by

$$V = \sum_{n=0}^{k}\sum_{m=0}^{n} \frac{\epsilon_{nm}}{2(n+1)} A_{nm}^2, \qquad (9)$$

where $\varepsilon_{nm} = 2$ for $2m = n$, and $\varepsilon_{nm} = 1$ for $2m \neq n$.

An alternate representation of a wavefront is in terms of monomials, i.e., powers of x and y, where $x = r\cos\theta$ and $y = r\sin\theta$. This representation is

$$W(x,y) = \sum_{n=0}^{k}\sum_{m=0}^{n} B_{nm} x^m y^{n-m}. \qquad (10)$$

The relationship between the Zernike polynomials and the monomials is

$$R_n^{n-2m} \begin{Bmatrix}\sin\\ \cos\end{Bmatrix} (n-2m)\theta = \sum_{i=0}^{q}\sum_{j=0}^{m}\sum_{k=0}^{m-j} (-1)^{i+j} \binom{|2m-n|}{2i+p} \binom{m-j}{k} \cdot \frac{(n-i)!}{j!(m-j)!(n-m-j)!} x^{n-2(i+j+k)-p} y^{2(i+k)+p}, \qquad (11)$$

where $p = 1$ for the sin terms, and $p = 0$ for the cos terms, and

$q = (2m - n)/2$ for the cos terms and n even,

$q = [(n - 2m)/2] - 1$ for the sin terms and n even,

$q = (2m - n - 1)/2$ for the cos terms and n odd,

$q = (n - 2m - 1)/2$ for the sin terms and n odd.

The quantity $\binom{i}{j}$ is the binomial factor defined by

$$\binom{i}{j} = i!/[(i-j)!j!]. \qquad (12)$$

Using these relationships, a matrix H can be defined that relates the coefficients of the Zernike polynomials to the coefficients of the monomials,[10]

$$\mathbf{B} = H\mathbf{A}, \qquad (13)$$

where B and A are the column vectors containing the coefficients of the monomials and Zernike polynomials, respectively. This approach is taken to simplify the procedure for obtaining the matrix relating the wavefront to the shearing data, since it is easier to obtain this matrix in terms of the monomials and then convert to Zernike polynomials using Eq. (13). Note that H is a square matrix of size N x N, where $N = (k + 1)(k + 2)/2$ for order k.

The relationship between the monomial coefficients of a wavefront B_{nm}, and the monomial coefficients of the corresponding x shear and y shear, C_{nm} and D_{nm}, is

$$C_{nm} = \sum_{j=1}^{k-n} \binom{j+m}{j} S^j B_{j+n,\,j+m},$$
$$D_{nm} = \sum_{j=1}^{k-n} \binom{j+n-m}{j} T^j B_{j+n,\,m}, \qquad (14)$$

where S and T are the shear values in the x and y directions, respectively. Note that if the wavefront is defined to order k, the shearing data are defined to order k - 1. Equation (14) defines two matrices, γ and δ, having dimensions M x N, where $M = k(k + 1)/2$.

The previously defined matrices, α and β, which relate the wavefront coefficients to the shearing coefficients for Zernike polynomials, may now be calculated in terms of γ, δ, and H. These are

$$\alpha = H_{k-1}^{-1}\gamma H_k,$$
$$\beta = H_{k-1}^{-1}\delta H_k, \qquad (15)$$

where the subscript on H indicates the order.

Explicit expressions for the elements of the matrices H, γ, and δ have not been written because it is more convenient, in writing a computer program, to work directly from Eqs. (11) and (14).

References

1. M. P. Rimmer, Appl. Opt. 13, 623 (1974).
2. J. B. Saunders and R. J. Bruening, Astron. J. 73,415 (1968).
3. D. Nyyssonen and J. M. Jerke, Appl. Opt. 12, 2061 (1973).
4. V. Ronchi, Appl. Opt. 3, 437 (1964).
5. A. Cornejo and D. Malacara, Appl. Opt. 9, 1897 (1970).
6. M. V. R. K. Murty and A. Cornejo, J. Opt. Soc. Am. 63, 1312 (1973).
7. J. C. Wyant, Appl. Opt. 12, 2057 (1973).
8. M. Born and E. Wolf, *Principles* of Optics (Pergamon, New York, 1964), p. 464.
9. D. Dutton et al., Appl. Opt. 7, 125 (1968).
10. H. Sumita, Jap. J. Appl. Phys. 8, 1027 (1969).